The 2023 World Congress on
Advances in Structural Engineering and Mechanics (ASEM23)
GECE, Seoul, Korea, August 16-18, 2023

Fluoride containing strontium substituted calcium mesoporous bioactive glass nanoparticles

*Parichart Naruphontjirakul[1)]

[1] *Biological Engineering Program, Faculty of Engineering, King Mongkut's University of Technology Thonburi, Bangkok, THAILAND*

[1)] *parichart.nar@kmutt.ac.th*

ABSTRACT

Monodispersed spherical fluoride containing strontium substituted calcium mesoporous bioactive glass nanoparticles (xSr-yF-MBGNs) with a hydrodynamic diameter range from 170 to 200 nm were successfully prepared using a microemulsion assisted sol-gel used a basic condition. A cationic surfactant (CTAB) was used to generate the mesopore structure pattern, a pore diameter of 8-10 nm. The particles were stable in aqueous solution as Zeta potential increased from -33 mV to -58 mV in the particle doping with F. F and Sr were incorporated into the MBGNs without altering physicochemical properties of the particles including size, morphology, pore size, and amorphous structure. In addition, xSr-yF-MBGNs at concentrations up to 1 mg/mL have no toxic effect on the hMSCs *in vitro*.

1. INTRODUCTION

Bioactive glass nanoparticles (BGNs) are indeed interested in various fields of application. BGNs have the ability to stimulate the regeneration and repair of damaged or diseased tissues, particularly in the field of bone and dental tissue engineering through the formation of a hydroxyapatite layer and the release of ions from the glass structure (Hench 2006). Due to their small size, BGNs have a large surface area-to-volume ratio, enhancing their reactivity and effectiveness (Naruphontjirakul 2016). Thus, BGNs can be incorporated into various biomaterials, including scaffolds, coatings, and composites, to impart bioactivity and enhance their overall performance (Zheng 2017).

Mesoporous bioactive glass nanoparticles (MBGNs) are a type of nanoscale material with a unique porous structure (2-50nm) and bioactive properties (El-Fiqi 2012). The highly ordered pore structure of MBGNs increased surface area and reactivity compared to bulk particles that can control drug delivery, ion release, and enhanced cellular interactions (Kang 2018). MBGNs were commonly synthesized through the sol-gel method that consisted of the hydrolysis and poly-condensation of precursor to form a colloidal in solution (sol) and simultaneously form a three-dimensional network (gel). To maintain the primary particles in the form of nanoparticles, a basic catalyst was used. A microemulsion-assisted sol-gel method was applied to achieve specific pore sizes

* Corresponding author, Assistant Professor (Ph.D.), Email: parichart.nar@kmutt.ac.th

and structures. Cetyltrimethylammonium bromide (CTAB), a cationic surfactant, played the role as a templating agent to generate the mesopore pattern (Liang 2015).

The composition of MBGNs can also be modified by incorporating different therapeutic elements to enhance bioactivity and promote specific biological responses. In recent years, different therapeutic ions, including strontium (Sr), zinc (Zn), copper (Cu), manganese (Mn), and fluoride (F) have been incorporated into MBGNs. Sr enhanced bone formation by activating osteoblast activity and inhibited bone resorption by inhibiting osteoclast activity (Fiorilli 2018). Zn had antimicrobial properties and upregulated the expression of the osteoblastic differentiation marker (Sun 2021). Cu stimulated osteogenesis and angiogenesis (Bari 2017). Mn influenced bone metabolism and activated osteoblast activity (Westhauser 2021). F balanced dentin and enamel demineralization/remineralization through the formation of fluoroapatite and inhibited the growth of acid-producing bacteria (Davis 2014). Therefore, the unique properties of MBGNs make them a promising candidate for applications in regenerative medicine, tissue engineering, drug delivery, and antimicrobial property.

The aim of this study was to synthesize and characterize F containing Sr substituted Ca MBGNs (xSr-yF-MBGNs) with a diameter size of 100-200 nm using the microemulsion-assisted sol-gel. The addition of fluoride ions to xSr-MBGNs could have the ability to promote the remineralization of teeth and prevent dental caries by enhancing the formation of fluorapatite, a more acid-resistant form of hydroxyapatite. xSr-yF-MBGNs could promote bone mineralization and strengthen bones and teeth. Thus, xSr-yF-MBGNs have the potential to improve oral health and enhance bone regeneration processes, making them a promising area of research in the field of biomaterials and nanomedicine.

2. MATERIALS AND METHODS

2.1 xSr-yF-MBGNs synthesis

To prepare xSr-yF-MBGNs, the microemulsion-assisted sol-gel under the basic condition was used. Briefly, 1.5 g of cetyltrimethylammonium bromide (CTAB Sigma–Aldrich, USA) was dissolved in 78 mL of pre-heated deionized water at 55°C in a 500 mL DURAN® bottle at a stirring rate of 600 rpm for 3 minutes at 55°C. Then, 24 mL of ethyl acetate (Sigma–Aldrich, USA) was added in the mixed solution. 16.8 mL of 2 M ammonium hydroxide solution (Sigma–Aldrich, USA) was added. 8.7 mL of tetraethyl orthosilicate (TEOS, Sigma–Aldrich, USA) was added and stirred for 30 minutes. Then calcium nitrate tetrahydrate (99%, Sigma–Aldrich, USA), strontium nitrate (99%, Sigma–Aldrich, USA), and sodium fluoride (≥99%, Sigma–Aldrich, USA) were weighed with the nominal ratio as shown in Table 1 and mixed. After 4 h of reaction, the formed colloidal particles were collected using centrifugation at 7380 rpm for 30 minutes. The particles were washed with DI water two times and ethanol two times before drying at 80 °C overnight and calcination at 700°C with a heating rate of 2°C/minute for 4 h.

2.2 xSr-yF-MBGNs characterization

Size and charge on the surface of particles were characterized by measuring the dynamic light scattering and zeta potential of a suspension, respectively (HORIBA, SZ-100Z2). The morphology and elemental components of the synthesised MBGNs were

investigated using emission scanning electron microscopy (SEM, JEOL, JSM-6610 LV, Japan). A specific surface area analyzer (BET, BELSORP-mini II, BEL, Japan) was used to investigate texture analysis. The functional groups and crystalline structure of the MBGNs was identified using Fourier transform infrared spectroscopy (FTIR; Thermo Scientific Nicolet iS5, USA) in attenuated total reflection (ATR) mode at a wavenumber ranging from 4000 to 600 cm^{-1} at a scan speed 32 scan/min with a resolution of 4 cm^{-1} and X-ray Diffractometer (XRD, Bruker AXS Model D8 Advance, Germany) using Cu Kα radiation (1.5406 A°) at 40KV/40mA. Data were collected in the 10–70° 2θ range with a step size of 0.02° and a dwell time of 0.5 s was used, respectively.

Table 1: Compositions of xSr-F-MBGNPs (nominal ratio)

	%mol			
	SiO_2	CaO	SrO	NaF
0Sr-0F-MBGNs	60	40	-	
50Sr-0F-MBGNs	60	20	20	
50Sr-1F-MBGNs	60	15	15	10
100Sr-0F-MBGNs	60	-	40	
100Sr-1F-MBGNs	60	-	30	10

2.3 Bioactivity

The bioactivity test was used to evaluate the formation of apatite on the surface of the particles soaked in the Simulated Body Fluid (SBF) solution (pH 7.4 at 37 °C). 50 mg of *xSr-yF-MBGNs* were incubated in 25 mL of SBF in a 50 mL centrifuge tube in an incubator shaker at 200 rpm, and 37 °C for 21 days. After 21 days, soaked *xSr-yF-MBGNs* were collected using centrifugation at 7380 rpm for 10 minutes. The formation of apatite was detected using SEM and EDS-SEM.

2.4 Cytotoxicity

The cytotoxicity effect of 0Sr-0F-MBGNs, 50Sr-0F-MBGNs, 50Sr-1F-MBGNs, 100Sr-0F-MBGNs, and 100Sr-1F-MBGNs against hMSCs was evaluated using MTT colorimetric assay (Thermo Fisher Scientific) according to the manufacturer's instructions. Human bone marrow-derived mesenchymal stem cells, hMSCs (ATCC® PCS-500-012™), were routinely cultured in α-MEM supplemented with 10% (v/v) fetal bovine serum (FBS, Thermo Fisher Scientific) (v/v), 100 U/mL antibiotic/antimycotic (Thermo Fisher Scientific) at 37 °C, 5% CO2 and in a fully humidified atmosphere. hMSCs were seeded in flat-bottomed 96-well plates (Corning) with a cell concentration of 5 x 10^4 cells/mL and allowed to attach in a monolayer overnight. The cells were treated with particles at concentrations ranging from 0–1 mg/mL: namely 0, 10, 100, 125, 250, 500, 750, and 1,000 µg/mL for 24 hours. Cell viability was determined using the MTT colorimetric assay based on the conversion of *3-(4,5*-dimethylthiazol-*2*-yl)-*2,5*-diphenyltetrazolium bromide (MTT) into formazan. Formazan is soluble in dimethyl sulfoxide (DMSO), and the concentration of soluble formazan was determined using a microplate reader (Infinite®200 Tecan, Austria) at 570 nm. The relative cell viability (% viability compared to the control (the untreated cells with the particles)) was calculated as a mean value ± standard error of the mean.

3. RESULTS AND DISCUSSIONS

The monodispersed MBGNs with a hydrodynamic diameter range from 170 to 200 nm were successfully synthesised through the microemulsion-assisted sol-gel process using 2M ammonium hydroxide as the base catalyst to control the size of the particles (Table 2). The calcination process at 700 °C for 4 hours was used to decompose and eliminate unreacted precursors and to incorporate therapeutic ions including Sr and F. The spherical shape and uniformity of xSr-yF-MBGNs were observed using SEM as shown in Figure1.

Table 2: Size and surface charge of xSr-yF-MBGNs

	Size (nm)	PDI	Zeta potential (mV)
0Sr-0F-MBGNs	181.87 ± 2.12	0.17 ± 0.03	-33.80 ± 0.40
50Sr-0F-MBGNs	177.60 ± 8.75	0.19 ± 0.01	-33.60 ± 0.56
50Sr-1F-MBGNs	182.17 ± 0.67	0.35 ± 0.03	-42.73 ± 0.65
100Sr-0F-MBGNs	186.87 ± 7.74	0.15 ± 0.03	-37.27 ± 0.35
100Sr-1F-MBGNs	197.73 ± 2.43	0.23 ± 0.04	-58.27 ± 0.47

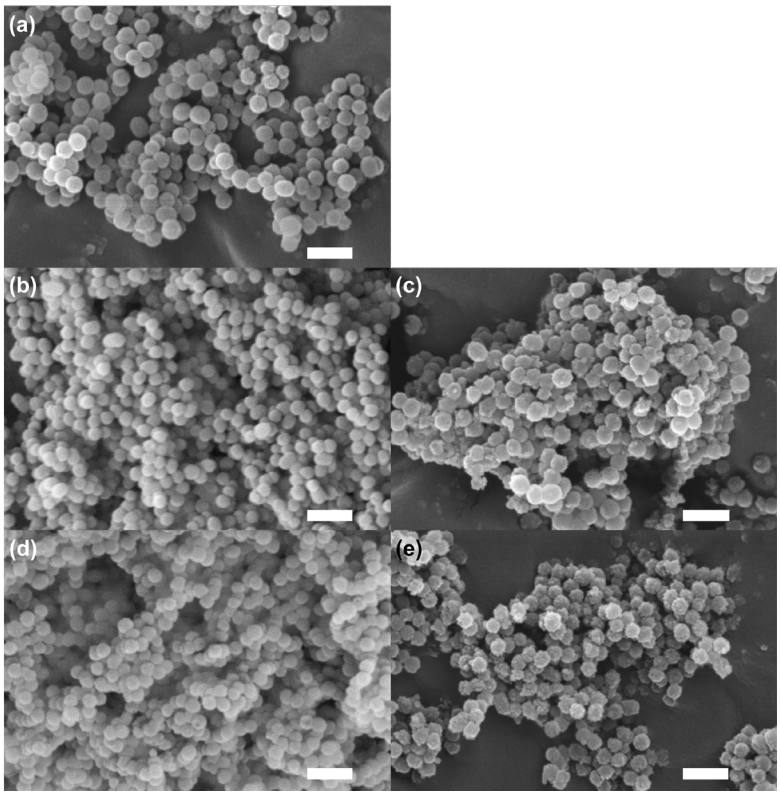

Fig. 1 SEM images of (a) 0Sr-0F-MBGNs, (b) 50Sr-0F-MBGNs, (c) 50Sr-1F-MBGNs, (d) 100Sr-0F-MBGNs, and (e) 100Sr-1F-MBGNs. Operate at 20 kV and 30 kX. Scale bar = 0.5 μm.

The XRD spectra of synthesised xSr-yF-MBGNs showed the broad halo band at 2Θ ~ 20-30º implying the amorphous nature. Sr and F were doped to 60SiO_2-40CaO binary glass system (0Sr-0F-MBGNs) without altering the amorphous structure (Figure 2 (a)). This disordered structure of amorphous nature can enhance solubility and accelerate dissolution rates (Jones 2001). The FTIR spectra showed the characteristic peak of the silica network at 800 cm^{-1} (symmetric Si-O-Si stretching) and 1000-1200 cm^{-1} (asymmetric Si-O-Si stretching) (Tabia 2019). The presence of Sr and F in the xSr-yF-MBGNs did not cause significant alteration to the chemical bonding of the particles.

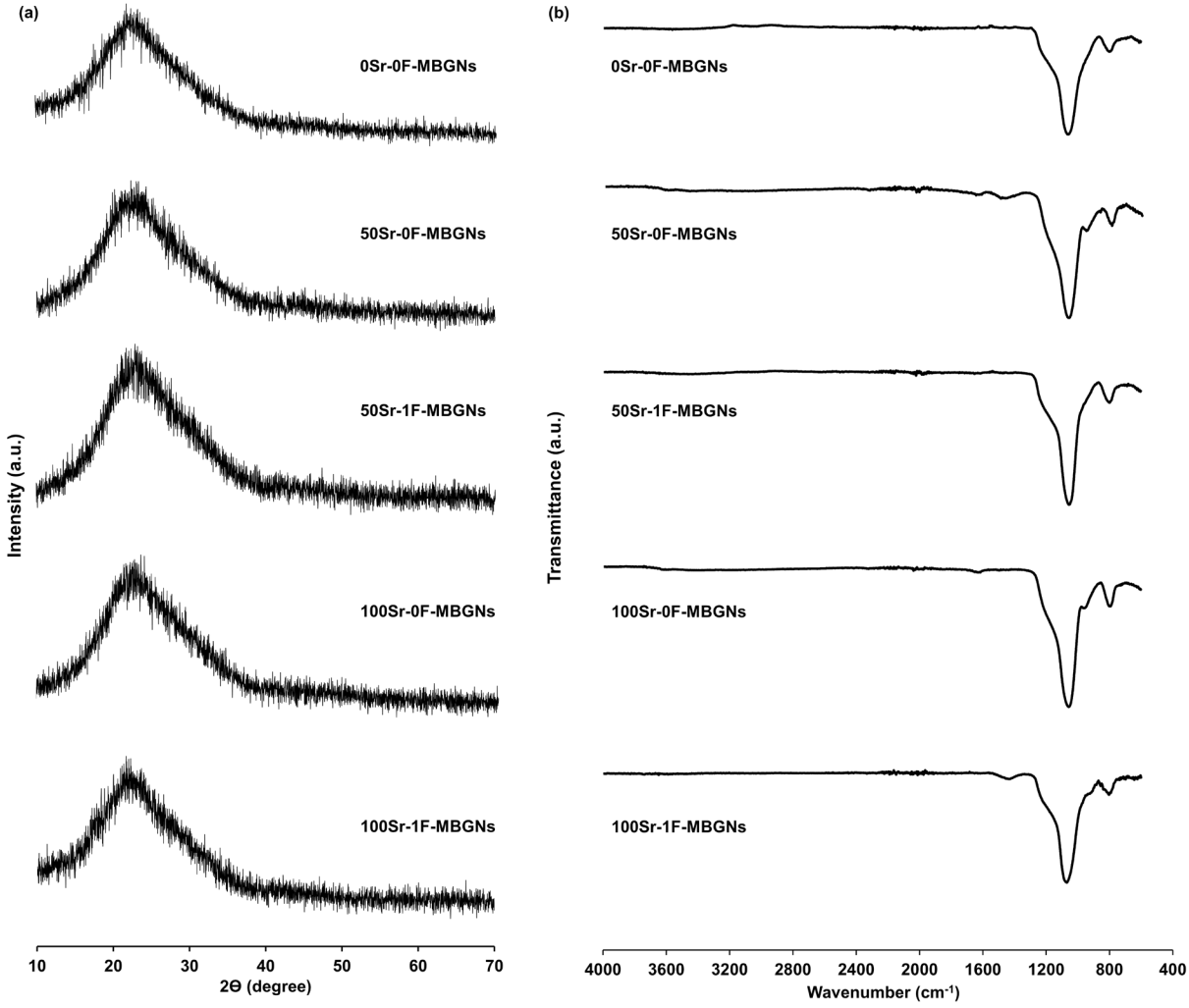

Fig. 2 (a) XRD and (b) FTIR spectra of 0Sr-0F-MBGNs, 50Sr-0F-MBGNs, 50Sr-1F-MBGNs, 100Sr-0F-MBGNs, and 100Sr-1F-MBGNs.

The specific surface area ($a_{s,BET}$), pore volume, and pore diameter of the particle did not significantly change when Sr and F were doped into the particle network (Table 3). The pore diameter of xSr-yF-MBGNs was in the range of 8-10 nm implying the mesoporous structure (ALOthman 2012). Taken together, these results indicated that

the incorporation of Sr and F did not significantly alter the physicochemical properties of MBGNs including chemical bonding of silica network, amorphous structure, specific surface area, pore volume, and pore diameter.

Table 3: BET Surface area analysis of xSr-yF-MBGNs

	$a_{s,BET}$ (m^2 g^{-1})	Pore volume (cm^3 g^{-1})	Pore diameter (nm)
0Sr-0F-MBGNs	131.2	0.38	9.22
50Sr-0F-MBGNs	137.3	0.43	9.61
50Sr-1F-MBGNs	140.7	0.31	8.84
100Sr-0F-MBGNs	148.4	0.37	9.31
100Sr-1F-MBGNs	153.6	0.32	8.75

The cytotoxicity effect of xSr-yF-MBGNs against hMSCs was evaluated using MTT assay to ensure their safety for biomedical applications. The relative cell viability of hMSCs exposed to xSr-yF-MBGNs up to the particle concentration at 1000 µg/mL was higher than 70% compared to the control (cells cultured in nanoparticles-free media) indicating the biocompatibility of the tested material (ISO 10993-5). Interestingly, metabolic cell activity of hMSCs exposed to 50Sr-0F-MBGNs statistically significantly increased at the concentration ≥ 750 µg/mL compared to the cells treated with alternative particles at the same concentration.

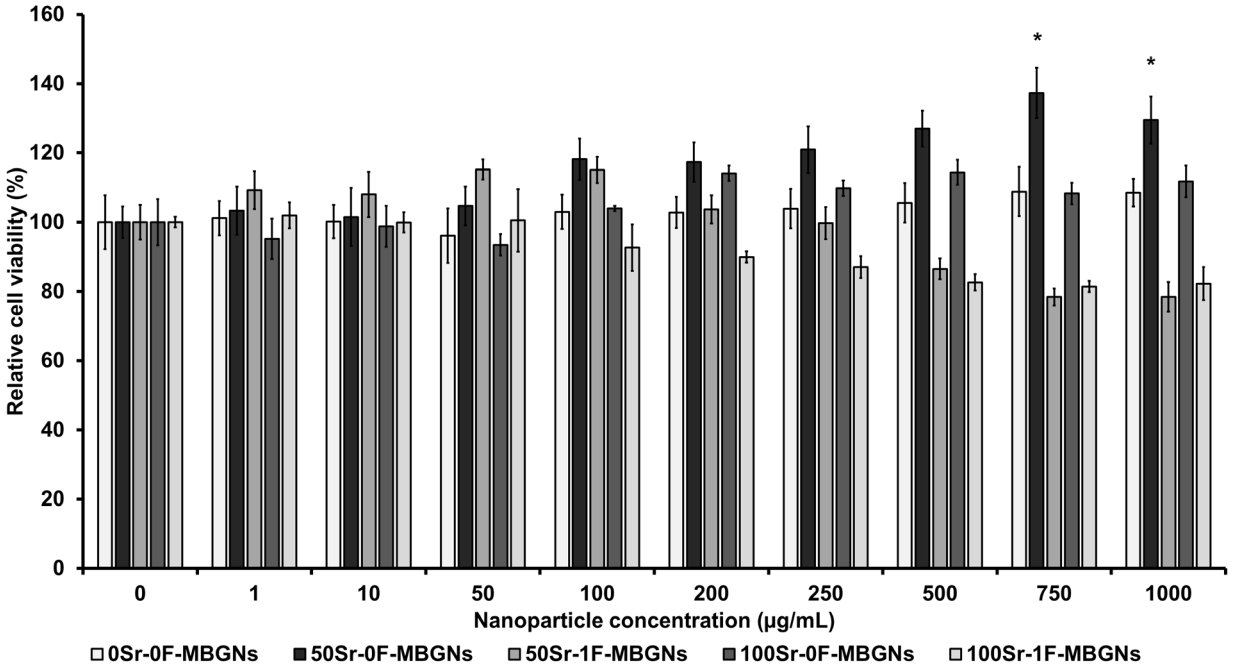

Fig. 3 Cell viability of hMSCs exposed to xSr-yF-MBGNs which were subtracted from the positive control (cells cultured in nanoparticles-free media). The data are expressed as mean ± SD of three independent experiments (n = 3). (*) indicates a statistically significant difference compared to controls ($p<0.05$).

4. CONCLUSIONS

xSr-yF-MBGNs were synthesised by combining the microemulsion-assisted sol-gel method and the heat treatment process. The monodisperse distribution xSr-yF-MBGNs had spherical morphology with the average particle size of 170 - 200 nm. Sr and F were successfully incorporated into $60SiO_2$-40CaO MBGNs while maintaining the original physicochemical characteristics of the particles, such as size, shape, pore size, and amorphous structure. xSr-yF-MBGNs with high specific surface area and uniform mesopores were biodegradable against hMSCs. To broaden further their therapeutic potential in bone-tissue and dental applications, additional investigations will be focused on the *in vitro* assessment of antibacterial effect, bioactivity, and osteogenic differentiation

ACKNOWLEDGMENTS

This research project was supported by Thailand Science Research and Innovation (TSRI) Basic Research Fund: Fiscal year 2023 under project number FRB660073/0164

REFERENCES

ALOthman, Z. A. (2012). A Review: Fundamental Aspects of Silicate Mesoporous Materials. *Materials*, *5*(12), 2874-2902. https://www.mdpi.com/1996-1944/5/12/2874

Bari, A., Bloise, N., Fiorilli, S., Novajra, G., Vallet-Regí, M., Bruni, G., Torres-Pardo, A., González-Calbet, J. M., Visai, L., & Vitale-Brovarone, C. (2017). Copper-containing mesoporous bioactive glass nanoparticles as multifunctional agent for bone regeneration. *Acta Biomaterialia*, *55*, 493-504. https://doi.org/https://doi.org/10.1016/j.actbio.2017.04.012

Davis, H. B., Gwinner, F., Mitchell, J. C., & Ferracane, J. L. (2014). Ion release from, and fluoride recharge of a composite with a fluoride-containing bioactive glass. *Dental Materials*, *30*(10), 1187-1194. https://doi.org/https://doi.org/10.1016/j.dental.2014.07.012

El-Fiqi, A., Kim, T.-H., Kim, M., Eltohamy, M., Won, J.-E., Lee, E.-J., & Kim, H.-W. (2012). Capacity of mesoporous bioactive glass nanoparticles to deliver therapeutic molecules. *Nanoscale*, *4*(23), 7475-7488.

Fiorilli, S., Molino, G., Pontremoli, C., Iviglia, G., Torre, E., Cassinelli, C., Morra, M., & Vitale-Brovarone, C. (2018). The incorporation of strontium to improve bone-regeneration ability of mesoporous bioactive glasses. *Materials*, *11*(5), 678.

Hench, L. L. (2006). The story of Bioglass. *J Mater Sci Mater Med*, *17*(11), 967-978. https://doi.org/10.1007/s10856-006-0432-z

Jones, J. R., Sepulveda, P., & Hench, L. L. (2001). Dose-dependent behavior of bioactive glass dissolution. *Journal of Biomedical Materials Research: An Official Journal of The Society for Biomaterials, The Japanese Society for Biomaterials,*

and The Australian Society for Biomaterials and the Korean Society for Biomaterials, *58*(6), 720-726.

Kang, M. S., Lee, N.-H., Singh, R. K., Mandakhbayar, N., Perez, R. A., Lee, J.-H., & Kim, H.-W. (2018). Nanocements produced from mesoporous bioactive glass nanoparticles. *Biomaterials*, *162*, 183-199. https://doi.org/https://doi.org/10.1016/j.biomaterials.2018.02.005

Liang, Q., Hu, Q., Miao, G., Yuan, B., & Chen, X. (2015). A facile synthesis of novel mesoporous bioactive glass nanoparticles with various morphologies and tunable mesostructure by sacrificial liquid template method. *Materials letters*, *148*, 45-49.

Naruphontjirakul, P., Greasley, S. L., Chen, S., Porter, A. E., & Jones, J. R. (2016). Monodispersed strontium containing bioactive glass nanoparticles and MC3T3-E1 cellular response. *Biomedical glasses*, *2*(1). https://doi.org/doi:10.1515/bglass-2016-0009

Sun, H., Zheng, K., Zhou, T., & Boccaccini, A. R. (2021). Incorporation of zinc into binary SiO2-CaO mesoporous bioactive glass nanoparticles enhances anti-inflammatory and osteogenic activities. *Pharmaceutics*, *13*(12), 2124.

Tabia, Z., El Mabrouk, K., Bricha, M., & Nouneh, K. (2019). Mesoporous bioactive glass nanoparticles doped with magnesium: drug delivery and acellular in vitro bioactivity. *RSC advances*, *9*(22), 12232-12246.

Westhauser, F., Wilkesmann, S., Nawaz, Q., Hohenbild, F., Rehder, F., Saur, M., Fellenberg, J., Moghaddam, A., Ali, M. S., Peukert, W., & Boccaccini, A. R. (2021). Effect of manganese, zinc, and copper on the biological and osteogenic properties of mesoporous bioactive glass nanoparticles. *Journal of Biomedical Materials Research Part A*, *109*(8), 1457-1467. https://doi.org/https://doi.org/10.1002/jbm.a.37136

Zheng, K., & Boccaccini, A. R. (2017). Sol-gel processing of bioactive glass nanoparticles: A review. *Advances in Colloid and Interface Science*, *249*, 363-373.